Electromagnetic Radiation Control for Nonlinear Dynamics of Hopfield Neural Networks

Wei Yao,[1, 2, 3] Jia Fang,[1] Fei Yu,[1] Li Xiong,[4] Lihong Tang,[5] Jin Zhang,[1, a)] and Yichuang Sun[6]
[1)]*School of Computer and Communication Engineering, Changsha University of Science & Technology, Changsha, 410114, Hunan, China*
[2)]*State Key Laboratory of Industrial Control Technology, Zhejiang University, 310058, Hangzhou, China*
[3)]*Key Laboratory of Computing and Stochastic Mathematics (Ministry of Education), School of Mathematics and Statistics, Hunan Normal University, Changsha, 410081, Hunan, China*
[4)]*School of Physics and Electromechanical Engineering, Hexi University, Zhangye, 734000, China*
[5)]*Software College, Changsha Social Work College, 410004, Changsha, China*
[6)]*School of Engineering and Computer Science, University of Hertfordshire, Hatfield AL10 9AB, UK*

(Dated: 21 June 2024)

Electromagnetic radiation (EMR) affects the dynamical behavior of the nervous system, and appropriate EMR helps to study the dynamic mechanism of the nervous system. This paper uses a sophisticated four-dimensional Hopfield neural network (HNN) model augmented with one or more memristors to simulate the effects of EMR. We focus on the chaotic dynamics of HNN under the influence of EMR. Complex dynamical behaviors are found and transient chaotic phenomena have the same initial value sensitivity, showing how transient chaos is affected by EMR. Multiperiodic phenomena induced by quasi-periodic alternations are found in the dual EMR, as well as the suppression properties of the dual EMR for system chaos. This implies that the dynamical behavior of the HNN system can be controlled by varying the amount of EMR or the number of affected neurons in the HNN. Finally, a strong validation of our proposed model is provided by Multisim and FPGA hardware.

Neurons in the human brain communicate through electrical and chemical signals, and these signals are subject to interesting chaotic phenomena when they are externally stimulated. We aim to build artificial neural networks and introduce external stimuli to study the dynamics of the neural networks when they are affected. We built a four-dimensional Hopfield neural network (HNN) and experimented with this problem using memristor-simulated electromagnetic radiation (EMR). As the number of EMRs increases, rich chaotic dynamics such as period, chaos, transient chaos, quasi-period, and multi-period are observed, which suggests that EMRs have a very significant effect on the HNN. In addition, we confirmed the theory by software simulation as well as hardware experiment. This study not only deepens our understanding of the dynamical behavior of brain neural networks but also provides more comprehensive insights into neuroscience and artificial intelligence, thus laying a solid foundation for future research and applications.

I. INTRODUCTION

The neural network system of the brain is a very complex biological system that serves as an organ for humans to carry out their thoughts, emotions, and behaviors. Its nervous system consists of neurons, and neurons communicate with each other through electrochemical signals, which can perform a variety of functions, such as information transfer and processing functions[1–3]. Factors such as uncertainty in information transfer between neurons, or external stimulation, can lead to nonlinear and complex dynamical behavior in the neural networks of the brain. Therefore, the study of the nonlinear dynamics of neural networks is necessary[4].

A neural network is a computational model inspired by the structure and function of the nervous system in the brain, where artificial neurons simulate the neural network of the brain[5]. Over the years, researchers have proposed various neural network models to simulate the dynamical behavior of biological nervous systems to better understand the mechanisms of chaos[6–13].

The Hopfield neural network(HNN) model was proposed by J.J. Hopfield in 1982[14]. In the field of artificial neural networks, the remarkable nonlinearity of the activation function endows HNNs with extraordinary capabilities in the representation of dynamical systems. As the weights of the neural synapses change, HNN can accurately represent the detailed features of chaotic attractors in complex bifurcation diagrams, Lyapunov exponents, and phase portraits, reflecting the rich dynamical behavior of the system state as a function of parameters. Therefore, HNN is widely used in nonlinear dynamics studies. For example, Chen et al.[15] utilized non-ideal memristive synapses to simulate electromagnetic-induced currents and constructed a four-dimensional memristive HNN model. They analyzed the complex dynamical behavior under different coupling strengths of memristive synapses. Similarly, Chen et al.[16] replaced the traditional hyperbolic function with a ReLU function as the activation function and investigated a three-neuron RHNN (ReLU-based HNN). They theoretically

[a)]mail_zhangjin@163.com

demonstrated its boundedness and stability and conducted numerical simulations on its complex chaotic dynamics. In addition, Chen et al.[17] proposed a novel RHNN model and revealed its complex dynamics via numerical measurements, indicating that the RHNN model can exhibit intricate and diverse dynamic characteristics.

The discipline of dynamics, from its humble beginnings as a branch field of physics, has developed into a vast interdisciplinary field. Benefiting from the rapid development of modern computer technology, computers have provided researchers with unprecedented convenience, enabling them to study nonlinear systems more efficiently. In this setting, neural network dynamics have rapidly risen as an emerging research field. Through mathematical modeling, computational simulation, data analysis, and theoretical analysis, this field is of great significance for understanding human brain functions, designing advanced artificial intelligence systems, and developing new neuroscience theories[18–21]. In recent years, there has been a surge of research on neural network dynamics, and in their study, Fatemeh et al.[22] examined the importance of higher-order interactions in the collective dynamics of the brain, in particular the effects of pairwise and three-body interactions on neuronal synchronization. It was found that even weak strengths of second-order interactions can promote synchronization at lower first-order coupling strengths. Majhi et al.[23] published a review of research on the behavior of higher-order network dynamics, exploring a variety of dynamical processes including synchronization phenomena, propagation processes, cooperative evolution, and consensus formation.

Based on exploring the nonlinear dynamics in HNN, a key element in understanding network nonlinearity is the concept of attractors. Attractors can range from simple to extremely complex, and it is this complexity that lies at the heart of chaos theory research. In the study of chaotic systems, attractors are divided into two main categories: trivial attractors and strange attractors[24–28]. A trivial attractor is a relatively simple form of attractor in a chaotic system, whose structure usually manifests as a point, a straight line, or a simple periodic orbit.[29] Although the dynamical behavior of the trivial attractors is relatively simple and there is predictability, it still plays an important role in chaotic systems. Singular attractors, also known as strange attractors, have extremely complex structures and non-periodic dynamical behaviors[30] and have been studied and applied in various scenarios[31–37], contrary to trivial attractors. From the point of view of the phase-plane diagram, the trajectory of the strange attractor is an irregular motion, presenting its highly complex, nonlinear, and chaotic character. A typical example is the Lorenz attractor[38,39]. In recent years, Lin et al. constructed a class of Lorenz-like Multivariate Weighted Chaotic Systems (MWCS) based on non-polynomial functions. They conducted a nonlinear dynamic analysis of the system and explored its application in image encryption[40].

According to the above description, the nonlinear properties in the original HNN are primarily manifested in the synaptic weights. These variations in weights are analogous to synaptic changes within the neural systems of the human brain[41–43]. But at the same time, we all know that from the neuron point of view, adding some external stimuli to the neuron will lead to some unexpected changes in the neuron, that is to say, these external stimuli can directly affect the neuron behavior and the state of the whole neural network[44–47]. In 2016, LV et al. first proposed the Hindmarsh-Rose neuron model by introducing a combination of magnetic flux and memristive current as an external stimulus[48]. Thereafter, there has been a surge in research on the memristive neuron model. Electromagnetic Radiation (EMR) is one of the external stimuli, that activates the neural network through electromagnetic waves generated by the interaction of electricity and magnetism. In recent years, the research on the influence of external stimuli such as EMR on neural networks has opened up new directions for the nonlinear dynamics of neural networks. Wan et al. established a three-neuron-based HNN. They introduced electromagnetic induction or bias current into the other two neurons under the influence of a single EMR. They found that, with the variation of memristor coupling strength, the HNN could exhibit complex dynamical behaviors[49,50]. Similarly, Lin et al. also constructed a three-neuron neural network under EMR. They discovered that a neural network with periodic attractors could generate numerous chaotic attractors by applying EMR to one of its neurons. Furthermore, they found that when this neuron simultaneously received stimulation from EMR and multi-layer logic pulses, the neural network could produce multiple-scroll attractors[51,52].

Therefore, it is extremely challenging and important to deeply study the nonlinear dynamical behaviors of brain neural networks and the mechanism of external stimuli affecting them[53–55]. Through in-depth understanding and exploration of the complex behavior of neural networks, we can provide more comprehensive knowledge and insights into the fields of neuroscience and artificial intelligence, thus laying a solid foundation for future research and applications.

Inspired by the above considerations, this paper establishes a four-dimensional HNN. A memristor is utilized to simulate EMR, serving as an external stimulus for the HNN. EMR interference is applied to the first and second neurons of the HNN. Through simulation experiments in Matlab, employing mathematical methods such as bifurcation diagrams, Lyapunov exponents, time domain waveform diagrams, Poincaré maps, and phase portraits, we have observed a rich variety of dynamical behaviors in the HNN system, including period, transient chaos, and multiperiod. It was also found that minor variations in the initial state can affect the dynamics of transient chaos. This indicates that EMR has a significant impact on the HNN.

The rest of the paper is organized as follows. Section II establishes the model of the HNN under varying amounts of EMR stimulation and conducts a stability analysis of its equilibrium point. Section III employs a series of mathematical analyses to embody the dynamical behavior of the HNN system. In section IV, the circuit is validated through experimental simulations using software and hardware implementations. Section V summarizes the work.

II. NEURAL NETWORK MODEL UNDER DIFFERENT AMOUNTS OF EMR STIMULATION

A. Mathematical model description

HNN is often defined as a network that closely resembles the structure of a biological nervous system and is a reliable model for simulating the dynamic activity of the brain. The following is an expression for a HNN model containing n neurons[56]:

$$C_i\dot{x}_i = -\mathrm{x}_i/R_i + \sum_{j=1}^{n}(w_{ij}\cdot f_i) + I_i \tag{1}$$

where C_i, x_i, and R_i denote the capacitance, voltage, and resistance inside and outside the cell membrane of the ith neuron, respectively. w_{ij} is the connection strength between neuron i and neuron j. f_i is the activation function, and since the adopted activation function is usually an S-type function with upper and lower limits, the activation function used in this paper is the *tanh* function. The last I_i denotes the input bias current.

In this paper, a memristor model is used to simulate EMR as an external stimulus to a four-dimensional HNN[57]. Based on the characteristics of the mathematical model of the memristor and Ohm's law, the memristor model in Eq. 2 is proposed, namely

$$\begin{cases} i = W(\varphi)v \\ d\varphi/dt = g(\varphi,v) \\ W(\varphi) = \rho\left(\alpha+3\beta\varphi^2\right) \\ g(\varphi,v) = \mu v+\varepsilon\varphi \end{cases} \tag{2}$$

Among them, i, v, and φ are current, voltage, and magnetic flux, respectively, while $W(\varphi)$ is the memory conductance, and the other parameters α, β, ρ, μ, and ε denote the adjustable parameters of the memristor model of EMR.

It is further verified below that the model is a characteristic of the memristor model. In this paper, the parameter ε is fixed to a value of 0, and a sinusoidal excitation is applied to the memristor model to obtain Eq. 3, which is

$$\begin{cases} V = A\sin(F*t) \\ I = \rho\left(\alpha+3\beta\varphi^2\right)*V \\ d\varphi/dt = \mu V \end{cases} \tag{3}$$

where A and F denote the amplitude and frequency of the sinusoidal stimulus, respectively. When the parameters are fixed as α=1, β=1, ρ=2, μ=1 and A=1, F is 1, 3, 6, respectively, as shown in Fig. 1, it can be seen that the model has three fingerprints of a memristor, each of them forms a hysteresis loop and passes through the origin, and they are progressively linear with increasing frequency. In this study, a four-dimensional HNN model is constructed and the values of the synaptic weights of the four-dimensional HNN are set to appropriate weights. Additionally, the EMR model affects the first neuron to form the model in the first case. Meanwhile, based on the first model, we add an EMR stimulation with the same parameters in the second neuron. To explore their dynamical behavior, the physical model of HNN under EMR is shown in Fig. 2.

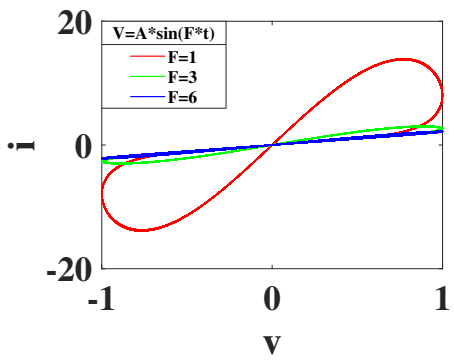

FIG. 1: Hysteresis loops of the memristor model at A=1, F=1;F=3;F=6.

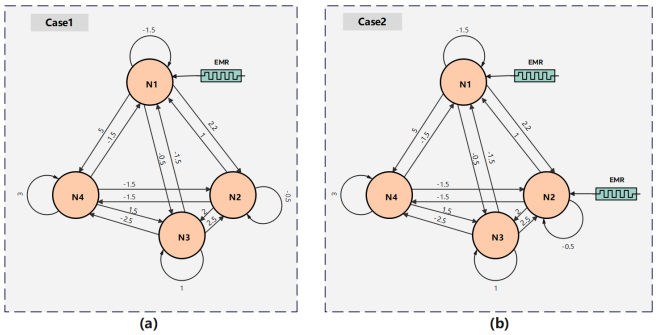

FIG. 2: HNN model under different EMR. (a)single EMR, (b)dual EMR.

Case 1: Under a single EMR, Eq. 1 and Eq. 2 are combined to obtain an HNN model with a single EMR as follows:

$$\begin{cases} \dot{x_1} = -x_1 - 1.5\tanh(x_1) + \tanh(x_2) \\ \qquad -1.5\tanh(x_3) - 1.5\tanh(x_4) \\ \qquad +\rho\left(\alpha+3\beta\varphi^2\right)x_1 \\ \dot{x_2} = -x_2 + 2.2\tanh(x_1) - 0.5\tanh(x_2) \\ \qquad +2.5\tanh(x_3) - 1.5\tanh(x_4) \\ \dot{x_3} = -x_3 - 0.5\tanh(x_1) + 1.4\tanh(x_2) \\ \qquad +\tanh(x_3) + 1.5\tanh(x_4) \\ \dot{x_4} = -x_4 + 5\tanh(x_1) - 1.5\tanh(x_2) \\ \qquad -2.5\tanh(x_3) + 3\tanh(x_4) \\ \dot{\varphi} = \mu x_1 \end{cases} \tag{4}$$

where $x_i(i=1,2,3,4)$, φ are the state variables of the system.

Case 2: The HNN model is obtained under dual EMR as

follows:

$$\begin{cases} \dot{x_1} = -x_1 - 1.5\tanh(x_1) + \tanh(x_2) \\ \qquad -1.5\tanh(x_3) - 1.5\tanh(x_4) \\ \qquad +\rho\left(\alpha + 3\beta\varphi_1^2\right)x_1 \\ \dot{x_2} = -x_2 + 2.2\tanh(x_1) - 0.5\tanh(x_2) \\ \qquad +2.5\tanh(x_3) - 1.5\tanh(x_4) \\ \qquad +\rho\left(\alpha + 3\beta\varphi_2^2\right)x_2 \\ \dot{x_3} = -x_3 - 0.5\tanh(x_1) + 1.4\tanh(x_2) \\ \qquad +\tanh(x_3) + 1.5\tanh(x_4) \\ \dot{x_4} = -x_4 + 5\tanh(x_1) - 1.5\tanh(x_2) \\ \qquad -2.5\tanh(x_3) + 3\tanh(x_4) \\ \dot{\varphi_1} = \mu_1 x_1 \\ \dot{\varphi_2} = \mu_2 x_2 \end{cases} \tag{5}$$

where $x_i (i = 1,2,3,4)$, φ_1 and φ_2 are the state variables of the system.

B. Stability analysis

In this paper, a combination of image and numerical analysis methods are used to analyze the stability of the model. For Case 1, making all the values on the left side of the equation be 0, Eq. 4 becomes as follows:

$$\begin{cases} 0 = -x_1 - 1.5\tanh(x_1) + \tanh(x_2) \\ \qquad -1.5\tanh(x_3) - 1.5\tanh(x_4) \\ \qquad +\rho\left(\alpha + 3\beta\varphi^2\right)x_1 \\ 0 = -x_2 + 2.2\tanh(x_1) - 0.5\tanh(x_2) \\ \qquad +2.5\tanh(x_3) - 1.5\tanh(x_4) \\ 0 = -x_3 - 0.5\tanh(x_1) + 1.4\tanh(x_2) \\ \qquad +\tanh(x_3) + 1.5\tanh(x_4) \\ 0 = -x_4 + 5\tanh(x_1) - 1.5\tanh(x_2) \\ \qquad -2.5\tanh(x_3) + 3\tanh(x_4) \\ 0 = \mu x_1 \end{cases} \tag{6}$$

Since μ is the intensity coefficient associated with EMR, whose value is specified here to be non-zero, it can be induced that x_1 is 0, i.e., Eq. 6 leads to Eq. 7:

$$\begin{cases} 0 = \tanh(x_2) - 1.5\tanh(x_3) - 1.5\tanh(x_4) \\ 0 = -x_2 - 0.5\tanh(x_2) + 2.5\tanh(x_3) - 1.5\tanh(x_4) \\ 0 = -x_3 + 1.4\tanh(x_2) + \tanh(x_3) + 1.5\tanh(x_4) \\ 0 = -x_4 - 1.5\tanh(x_2) - 2.5\tanh(x_3) + 3\tanh(x_4) \end{cases} \tag{7}$$

From Eq. 7 we have:

$$\tanh(x_2) = 1.5\tanh(x_3) + 1.5\tanh(x_4) \tag{8}$$

Substituting Eq. 8 into Eq. 7 yields Eq. 9:

$$\begin{aligned} x_2 = &-0.5\left(1.5\tanh(x_3) + 1.5\tanh(x_4)\right) \\ &+2.5\tanh(x_3) - 1.5\tanh(x_4) \end{aligned} \tag{9}$$

We can obtain the solutions of x_3 and x_4 from the following two equations:

$$\begin{cases} 0 = -x_3 + 1.4\tanh(1.75\tanh(x_3) - 2.25\tanh(x_4)) \\ \qquad +1\tanh(x_3) + 1.5\tanh(x_4) \\ 0 = -x_4 - 1.5\tanh(1.75\tanh(x_3) - 2.25\tanh(x_4)) \\ \qquad -2.5\tanh(x_3) + 3\tanh(x_4) \end{cases} \tag{10}$$

Denote x_3 in terms of x and x_4 in terms of y. The numerical implicit function for the equilibrium point of Case 1 can be obtained:

$$\begin{cases} H_1(x,y) = -x + 1.4\tanh(1.75\tanh(x) - 2.25\tanh(y)) \\ \qquad +1\tanh(x) + 1.5\tanh(y) = 0 \\ H_2(x,y) = -y - 1.5\tanh(1.75\tanh(x) - 2.25\tanh(y)) \\ \qquad -2.5\tanh(x) + 3\tanh(y) = 0 \end{cases} \tag{11}$$

The numerical plots of the Eq. 11 are shown in Fig.3. It

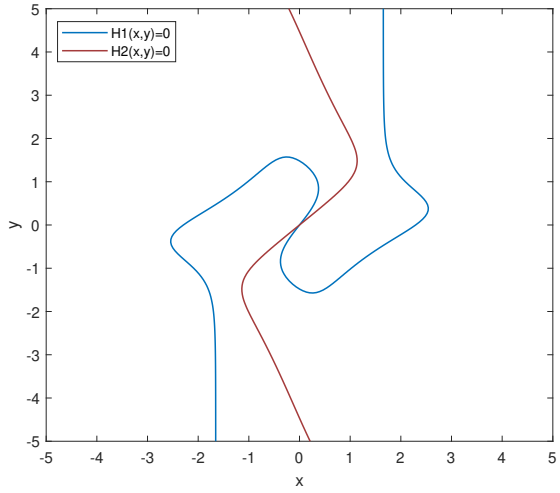

FIG. 3: Equilibrium point of Case 1.

is clear that the system is in the equilibrium point state when $x_1 - x_4$ are all 0. According to Eq. 6, it can be known that the value of φ will not affect the equilibrium point of the model, therefore, φ can be considered to be an arbitrary value. An infinite number of equilibrium points can be obtained, that is, $(0,0,0,0,\varphi)$. When the values of the state variables $x1, x2, x3, x4$ are fixed to zero in all other dimensions, only φ is free to vary throughout its domain of definition. A 1-dimensional trajectory is formed in the 5-dimensional space, which corresponds to the equilibrium line of system (4).

It is well known that in nonlinear systems, the equilibrium point is the point at which the system does not change in some state. By linearizing the system and calculating the Jacobi matrix at the equilibrium point, the stability of the equilibrium point of the system can be analyzed in terms of eigenvalues.

Before that, it is necessary to determine the parameters related to EMR, which are set in this study as follows: ρ=2, α=1, β=-1, and μ=1. Therefore, the relevant Jacobi matrix can be obtained as:

$$\mathrm{J} = \begin{bmatrix} -0.5-6\varphi^2 & 1 & -1.5 & -1.5 & 0 \\ 2.2 & -1.5 & 2.5 & -1.5 & 0 \\ -0.5 & 1.4 & 0 & 1.5 & 0 \\ 5 & -1.5 & -2.5 & 2 & 0 \\ 1 & 0 & 0 & 0 & 0 \end{bmatrix} \tag{12}$$

Taking the vector $v = [0,0,0,0,1]^T$, then there is $Jv = 0v$, therefore 0 is an eigenvalue. A change in the value of φ does not affect the Jacobi matrix of the system to produce 0 eigenvalues. When an eigenvalue with zero real parts exists, the stability of the equilibrium point can not be directly concluded. In this case, further analysis is required to determine the stability of the system.

For Case 2, in the same way as Case 1, setting all the values on the left side of Eq. 5 to 0 we can obtain the equilibrium point equation as follows:

$$\begin{cases} 0 = -x_1 - 1.5\tanh(x_1) + \tanh(x_2) \\ \quad -1.5\tanh(x_3) - 1.5\tanh(x_4) \\ \quad +\rho\left(\alpha + 3\beta\varphi_1^2\right)x_1 \\ 0 = -x_2 + 2.2\tanh(x_1) - 0.5\tanh(x_2) \\ \quad +2.5\tanh(x_3) - 1.5\tanh(x_4) \\ \quad +\rho\left(\alpha + 3\beta\varphi_2^2\right)x_2 \\ 0 = -x_3 - 0.5\tanh(x_1) + 1.4\tanh(x_2) \\ \quad +\tanh(x_3) + 1.5\tanh(x_4) \\ 0 = -x_4 + 5\tanh(x_1) - 1.5\tanh(x_2) \\ \quad -2.5\tanh(x_3) + 3\tanh(x_4) \\ 0 = \mu_1 x_1 \\ 0 = \mu_2 x_2 \end{cases} \tag{13}$$

It is easy to see that x_1 and x_2 are both 0, which leads to Eq. 14:

$$\begin{cases} 0 = -1.5\tanh(x_3) - 1.5\tanh(x_4) \\ 0 = 2.5\tanh(x_3) - 1.5\tanh(x_4) \\ 0 = -x_3 + \tanh(x_3) + 1.5\tanh(x_4) \\ 0 = -x_4 - 2.5\tanh(x_3) + 3\tanh(x_4) \end{cases} \tag{14}$$

Denote x_3 in terms of x and x_4 in terms of y. The numerical implicit function for the equilibrium point of Case 2 can be obtained:

$$\begin{cases} H_1(x,y) = -1.5\tanh(x) - 1.5\tanh(y) = 0 \\ H_2(x,y) = 2.5\tanh(x) - 1.5\tanh(y) = 0 \\ H_3(x,y) = -x + \tanh(x) + 1.5\tanh(y) = 0 \\ H_4(x,y) = -y - 2.5\tanh(x) + 3\tanh(y) = 0 \end{cases} \tag{15}$$

Eq. 15 is plotted as in Fig. 4, and it is clear that the equation holds when x_3 and x_4 are also zero. According to Case1, it is also possible to obtain that φ_1 and φ_2 are arbitrary values. In this 2-dimensional space, all combinations of φ_1 and φ_2 form a surface, and each point on this surface can represent an equilibrium state within the 6-dimensional space. Therefore, this set naturally forms an equilibrium surface for system (5). Since φ_1 and φ_2 can vary independently, the system can achieve equilibrium at any point on the φ_1-φ_2 surface, thereby enhancing the diversity of equilibrium states.

In order to investigate the effect of EMR on the equilibrium points of the system, the HNN without the EMR is calculated and validated. A system of nonlinear equations is iterated and solved using the fsolve() function in Matlab to obtain three equilibrium points of the HNN without EMR, which are E1(0, 0, 0, 0), E2(-0.7673, -2.4927, -0.2072, 0.8744), E3(0.7673, 2.4927, 0.2072, -0.8744).

Since the value of φ is taken arbitrarily, then it can be assumed that the equilibrium points of this HNN have changed from a finite number of three equilibrium points, to an infinite number of them, with the addition of the memristor. It shows that the addition of the EMR memristor model makes the HNN produce richer and more complex dynamical behaviors. This finding provides a solid foundation for us to explore in depth the dynamical changes induced by the memristor in the HNN, so we use more mathematical methods and mathematical tools to analyze these complex dynamical behaviors in more detail.

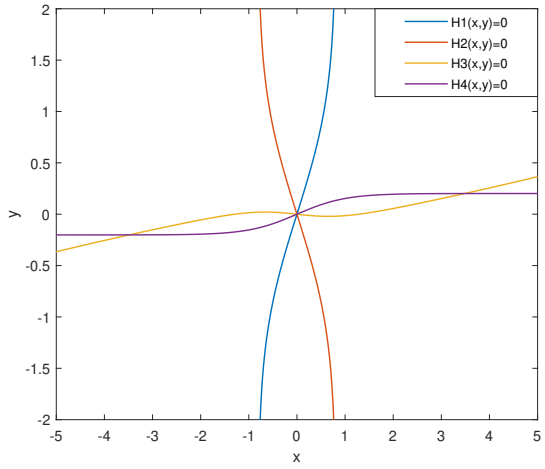

FIG. 4: Equilibrium point of Case 2.

III. ANALYSIS OF THE DYNAMICAL BEHAVIOR OF HNN UNDER THE INFLUENCE OF DIFFERENT AMOUNTS OF EMR

The objective of this section is to analyze the enriched dynamical behavior of the HNN model under the influence of different amounts of EMR. A variety of numerical studies are performed for this purpose, including bifurcation diagrams, Lyapunov exponents, time domain waveform diagrams, Poincaré maps, and phase portraits[58]. Bifurcation diagrams are very intuitive and effective tools for visualizing the change and evolution of the system behavior. The Lyapunov exponents are an important tool for describing and evaluating the chaotic behavior of nonlinear dynamical systems, i.e., a

metric to quantify the chaotic properties of nonlinear dynamical systems, reflecting the rate of separation of neighboring trajectories. Time domain waveform diagrams show the signal waveforms of the parameters in the system in time. The phase portrait is more intuitive to the record of the system trajectory. Each of the above numerical features is simulated by Matlab R2017b and is computed using the Lunger-Kutta algorithm.

A. Dynamical behavior under single EMR

An attractor usually behaves as a result of the convergence of all neighboring trajectories in a set[58]. In the study, the dynamical behavior of the system under the condition that the parameters of the memristor are varied shows convergence.

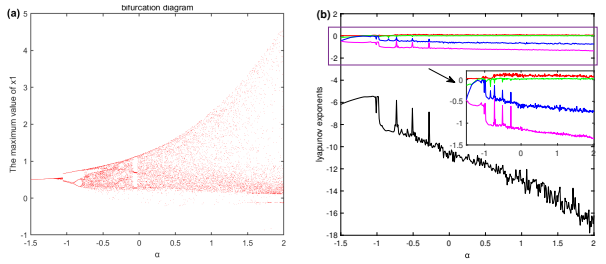

FIG. 5: The α-dependent dynamics with ρ=2, β=-1 and μ=1. (a) Bifurcation diagram under initial states (0.1,0,0,0,0), (b) Lyapunov exponents under initial states (0.1,0,0,0,0).

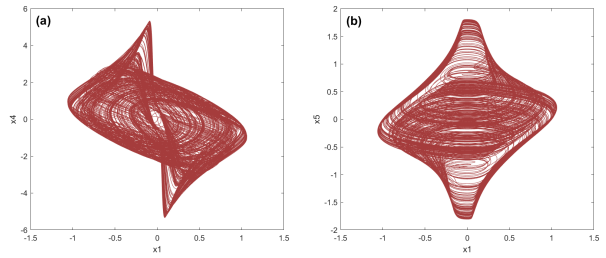

FIG. 6: Phase portrait of the HNN under EMR with α=-0.15, ρ=2, β=-1, μ=1, initial states $(x_1,x_2,x_3,x_4,\varphi) = (0.1,0,0,0,0)$. (a) $x_1 - x_3$, (b) $x_1 - x_5$.

First, the parameters α of the memristor model of EMR acted as variable parameters. The variable range of the α is [-1.5, 2], the other parameters are ρ=2, β=-1, μ=1, and the initial values $(x_1,x_2,x_3,x_4,\varphi) = (0.1,0,0,0,0)$. The dynamical behaviors of the HNN under different EMRs are investigated, and Fig. 5(a) shows the EMR parameter bifurcation diagram of the HNN under different α, and Fig. 5(b) shows the Lyapunov exponents. From the bifurcation diagram and the Lyapunov exponents, it can be known that for the parameter α at -0.85, the system has an obvious chaos phenomenon. Taking the parameter of α = -0.15 as an example, the first four Lyapunov exponents are $LE_1 = 0.1043, LE_2 = 0.014, LE_3 = -0.5524, LE_4 = -1.106$. Based on the phase portrait in Fig. 6 combined with the definition of an attractor, it is known that the attractor is a chaotic attractor.

Transient chaos is also known as metastability chaos. Unlike conventional attractors, where the trajectory produced by chaos is a strange attractor, transient chaos initially looks like a strange attractor, but eventually, its initially unstable solution decays to an equilibrium point[58,59]. In the following, the transient chaos of HNN under the influence of a single EMR will be explored.

In order to see the difference between transient chaos and chaos more intuitively, the three dynamical behaviors of the model are given in Fig. 7, including the phase portraits and time domain waveforms of periodic, transient chaos, and chaos. When the parameter α = -0.8, it can be learned from the time domain waveform diagram in Fig. 7(a) and the phase portrait in Fig. 7(b) that the model is in a periodic state, and the motion trajectory approximates a closed track. When the parameter α = -0.7, the model is in transient chaos, see Fig. 7(c), Fig. 7(d), and when parameter α = 1, the model is in a chaotic state as shown in Fig. 7(e) and Fig. 7(f).

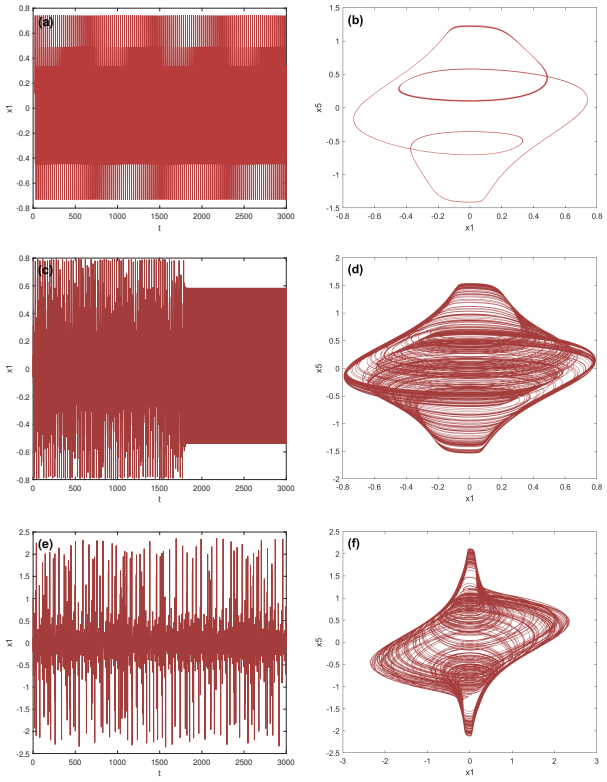

FIG. 7: Time domain waveforms and phase portraits of periods, transient chaos, and chaos under different α. (a) and (b) α= -0.8; (c) and (d) α = -0.7; (e) and (f) α =1.

Usually, the initial value sensitivity characteristics of chaotic phenomena are investigated in experiments. Yet, rarely there is a study on the initial value sensitivity characteristics of transient chaos as a dynamical behavior. In this study, the initial value sensitivity of transient chaotic phenomena is

investigated by time domain waveform diagrams, phase portraits, and Poincaré maps. Initial value variations affect the process of transforming chaos into periods of transient chaos. As can be seen from Fig. 8, the variation of different initial values directly affects the time at which the period appears. We change the initial value x_1 from 0.1 to 0.15, while keeping the rest of the initial values unchanged, and set the EMR memristor parameters α=-0.7, ρ=2, β=-1, and μ=1, respectively. This suggests that transient chaos is equally sensitive to initial values. The feature can also be visualized more intuitively through the phase portrait in Fig. 9. The different initial values in the figure are plotted by different colors, and it can be seen that each color is very distinct in the phase portrait with (x_5, x_3, x_2) as the axis. The corresponding conclusions can also be drawn from the Poincaré map in Fig. 10, where the individual values are represented by different colours. It shows that when the rest of the conditions are constant, small changes in the initial values can lead to differences in the values for each time.

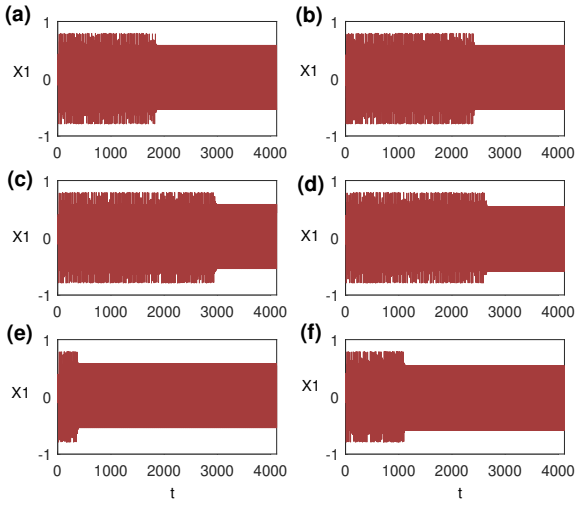

FIG. 8: Time domain waveforms of transient chaos at different initial values. (a) $(0.10,0,0,0,0,0)$, (b) $(0.11,0,0,0,0,0)$, (c) $(0.12,0,0,0,0,0)$, (d) $(0.13,0,0,0,0,0)$, (e) $(0.14,0,0,0,0,0)$, (f) $(0.15,0,0,0,0,0)$.

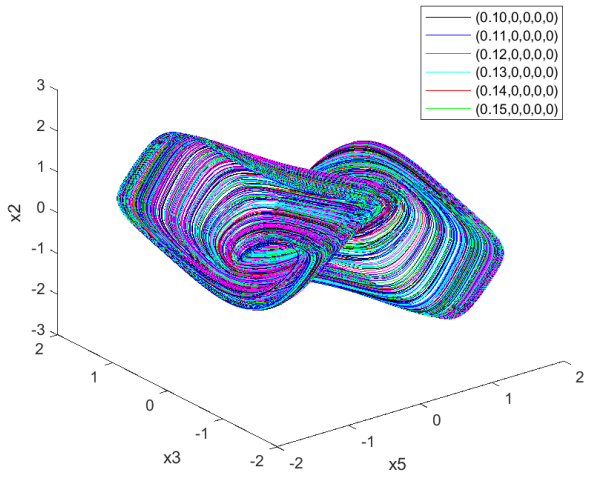

FIG. 9: Phase portrait of transient chaos at different initial states.

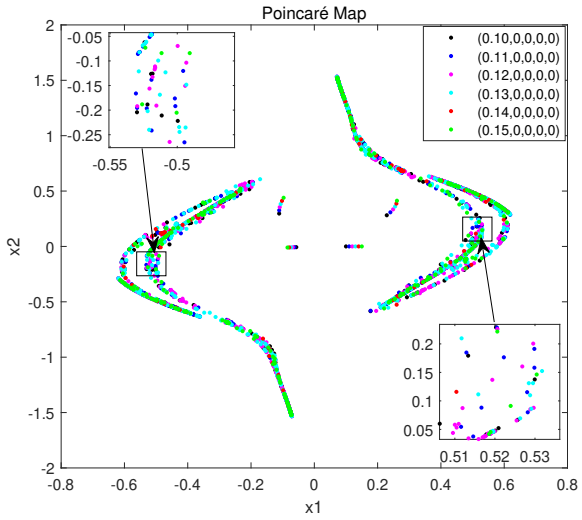

FIG. 10: Poincaré maps of transient chaos at different initial states.

B. Dynamical behavior under dual EMR

Quasi-periodic behavior describes in nonlinear dynamics theory a unique pattern of change in the state of a system over time that neither conforms to a strict periodic law nor falls into complete non-periodic chaos. This behavior exhibits the regularity and predictability that systems exhibit as they evolve through time while retaining a degree of complexity and non-repeatability.[60]. It has important theoretical research and application in the fields of nonlinear science and chaotic encryption.

Including a second EMR in the HNN system of Case 1 causes the chaos to be suppressed, leading to quasi-periodic behavior. All parameters in Case 1 keep constant and α=1. In Eq. 5, the parameters of the EMR memristor model are treated as variables. Specifically, the parameter α is allowed to vary within the range [-1,1.5], while the other parameters are set as follows: ρ = 2, β = -1, and μ_2 = 0.05. Initial values $(x_1, x_2, x_3, x_4, \varphi_1, \varphi_2) = (0.1, 0, 0, 0, 0, 0)$, and Fig. 11 shows the Lyapunov exponents of the HNN under different α. When the parameter α = 0.75, a Poincaré map is shown in Fig. 12, where the intersection of the model from positive to negative across the cross-section is recorded with the axis at x_4 = 0 to obtain a Poincaré cross-section. Its Lyapunov exponents are computed as $LE_1 = 0.01929$, $LE_2 = 0.004366$, $LE_3 = -0.02177$, $LE_4 = -0.07165$, $LE_5 = -3.291$ and $LE_6 = -13.69$. The positive Lyapunov exponents LE_1 and LE_2 im-

ply that the system exhibits sensitivity in certain dimensions, with even small changes in initial conditions being amplified over time. Similarly, the spatial alternation of quasi-periodic phenomena can be observed very intuitively through the time-domain waveform in Fig. 13. This peculiar phenomenon can be judged as a Multiperiodic phenomena resulting from the alternation of two quasi-periodic behaviors.

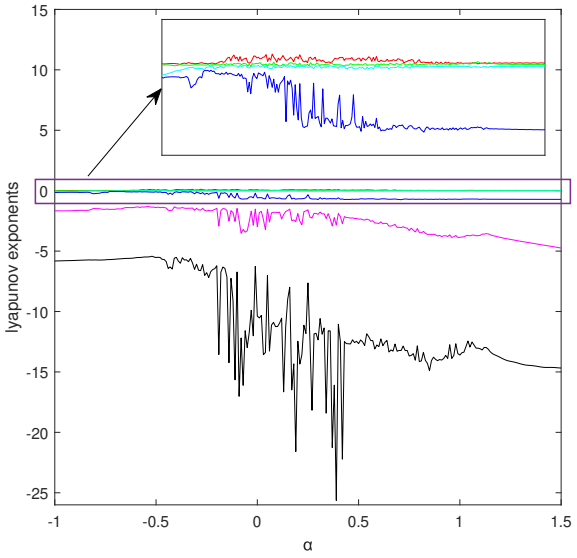

FIG. 11: The Lyapunov exponents under α-dependent dynamics with ρ=2, β=-1, μ_2=0.05 and initial states (0.1,0,0,0,0,0).

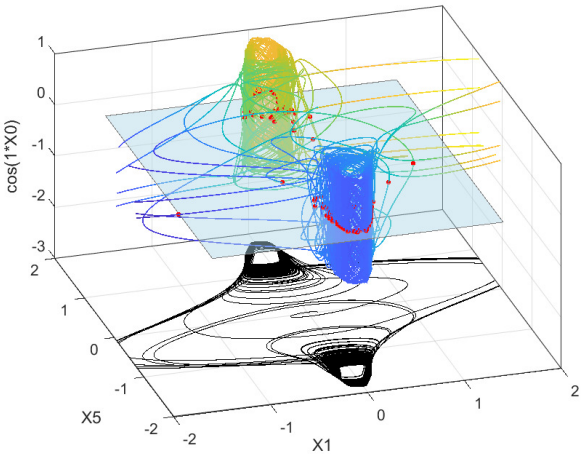

FIG. 12: Dynamics for $\alpha = 0.75$, the blue color in the space represents the Poincaré cross-section, while the black color represents the phase portrait for (x1, x5).

With the parameter settings of Case 1, fixing the variable α to 1 and keeping the other parameters constant, the effect of variation of the second EMR parameter μ_2 in Case 2 on the

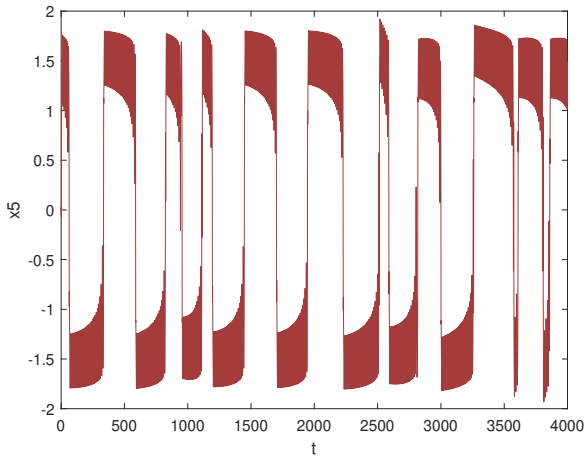

FIG. 13: Dynamics for $\alpha = 0.75$, Time domain waveforms of attractors.

system was explored. The Lyapunov exponential plot in Fig. 11 shows that the system exhibits a chaotic state at values of $-0.45, -0.15, 0.26$, and 0.5 for the parameter α, respectively. The $(x_1 - x_5)$ phase portraits for these four chaotic states are shown in Fig. 14. Using α as the system parameters at these chaotic states, the effect of the variation of μ_2 in the interval $[0, 1]$ on the maximum Lyapunov exponent of the system is analyzed. According to Fig. 15, the maximum Lyapunov exponent of the HNN shows a decreasing trend with the increase of μ_2 and finally stabilizes around 0.01. This phenomenon indicates that the second EMR can control the dynamical behavior of the system by regulating μ_2. It also shows that the μ_2 parameter can increase the stability and predictability of the chaotic system. Combining the results of Case 1 and Case 2 suggests that the EMR is able to both induce the HNN to generate a chaotic state and effectively inhibit that chaotic state. This finding provides a new theoretical basis for medical research on cerebral neurological diseases. Based on the study and analysis of the above system, it can be found that the stimulation of the four-dimensional HNN by different numbers of EMRs leads to changes in the dynamical behavior of the chaotic attractor, while unexpected dynamical behaviors occur under certain EMR memristor parameters, both chaotic and periodic. These dynamical behaviors under external stimuli are very interesting and deserve further investigation.

IV. CIRCUIT SIMULATION AND FPGA HARDWARE VERIFICATION

Because the mathematical model of the HNN as well as the memristor mathematical model can be implemented with commercial components, its circuit experimentation is equally important in practical engineering applications. It not only validates the numerical study of the above theoretical model but also means that the theoretical model can be fabricated and applied in reality. In this section, various dynamical behaviors

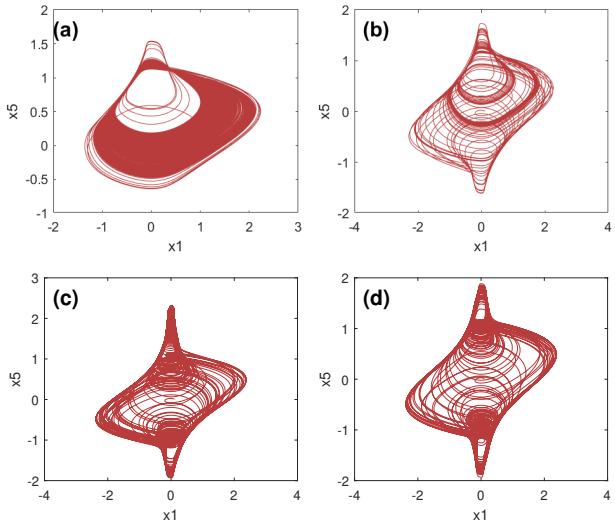

FIG. 14: Chaotic phase portrait with different α parameters. (a) α = -0.45, (b) α = -0.15, (c) α = 0.26, (d) α = 0.5.

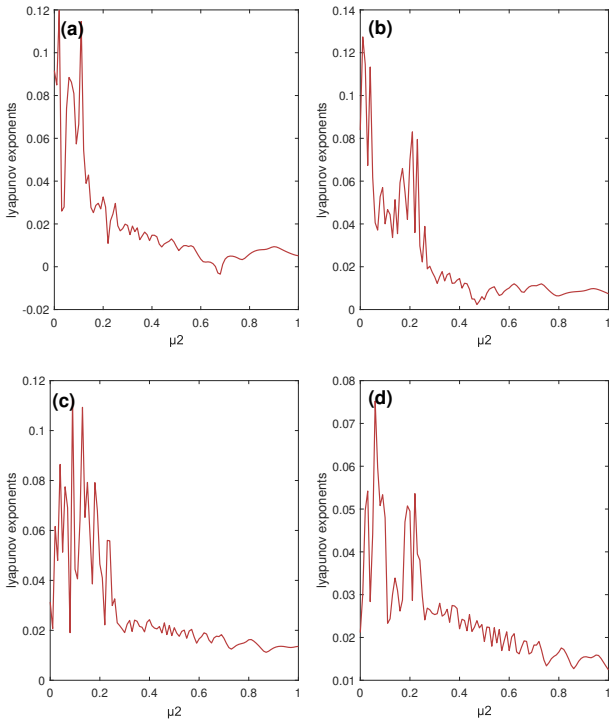

FIG. 15: Plot of the maximum Lyapunov exponent with parameter μ_2 when parameter α makes the system chaotic. (a) α = -0.45, (b) α = -0.15, (c) α = 0.26, (d) α = 0.5.

of the theoretical model are effectively verified by Multisim software as well as hardware simulations on FPGA.

Activation functions are required in neural network circuits, and a circuit design for a hyperbolic tangent function-tanh[61–63] is implemented using a pair of NPN transistors, two amplifiers, eight resistors, and a supply voltage V_{CC}. As shown in Fig. 16, where the parameters R = 10$k\Omega$, R_f =520Ω, R_C =1$k\Omega$, V_{CC} =15V, and I_0 =1.1mA. Its input-output equation can be written as $V_o = -tanh(V_i)$.

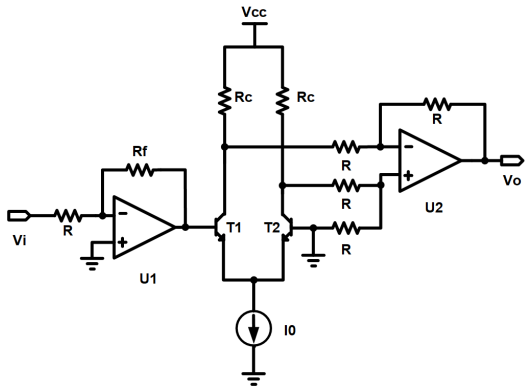

FIG. 16: Circuit design for tanh activation function.

Due to the characteristics of the model in this study, Case 2 adds EMR to the second neuron of Case 1, so the circuit validation is done by adding switches to the circuit model of Case 2. When the switch is fully closed, it represents the circuit under Case 2, and when the switch is fully open, it represents the circuit design of Case 1. According to Kirchhoff circuit law, the corresponding circuit state equation is shown by Eq. 14.

$$
\begin{cases}
RC\dfrac{dv_1}{dt} = -v_1 + \dfrac{R}{R_1}\tanh(v_1) + \dfrac{R}{R_2}\tanh(v_2) \\
\qquad + \dfrac{R}{R_3}\tanh(v_3) + \dfrac{R}{R_4}\tanh(v_4) \\
\qquad + R\left(-\dfrac{1}{R_5} + \dfrac{v_5^2}{R_6}\right)v_1 \\
RC\dfrac{dv_2}{dt} = -v_2 + \dfrac{R}{R_7}\tanh(v_1) + \dfrac{R}{R_8}\tanh(v_2) \\
\qquad + \dfrac{R}{R_9}\tanh(v_3) + \dfrac{R}{R_{10}}\tanh(v_4) \\
\qquad + R\left(-\dfrac{1}{R_{11}} + \dfrac{v_6^2}{R_{12}}\right)v_2 \\
RC\dfrac{dv_3}{dt} = -v_3 + \dfrac{R}{R_{13}}\tanh(v_1) + \dfrac{R}{R_{14}}\tanh(v_2) \\
\qquad + \dfrac{R}{R_{15}}\tanh(v_3) + \dfrac{R}{R_{16}}\tanh(v_4) \\
RC\dfrac{dv_4}{dt} = -v_4 + \dfrac{R}{R_{17}}\tanh(v_1) + \dfrac{R}{R_{18}}\tanh(v_2) \\
\qquad + \dfrac{R}{R_{19}}\tanh(v_3) + \dfrac{R}{R_{20}}\tanh(v_4) \\
RC\dfrac{dv_5}{dt} = -\dfrac{R}{R_{21}}v_1 \\
RC\dfrac{dv_6}{dt} = -\dfrac{R}{R_{22}}v_2
\end{cases}
\tag{16}
$$

The circuit design is shown in Fig. 17. The design can be divided into several modules connected with each other, described by Eq. 16, where RC is the circuit time constant in the

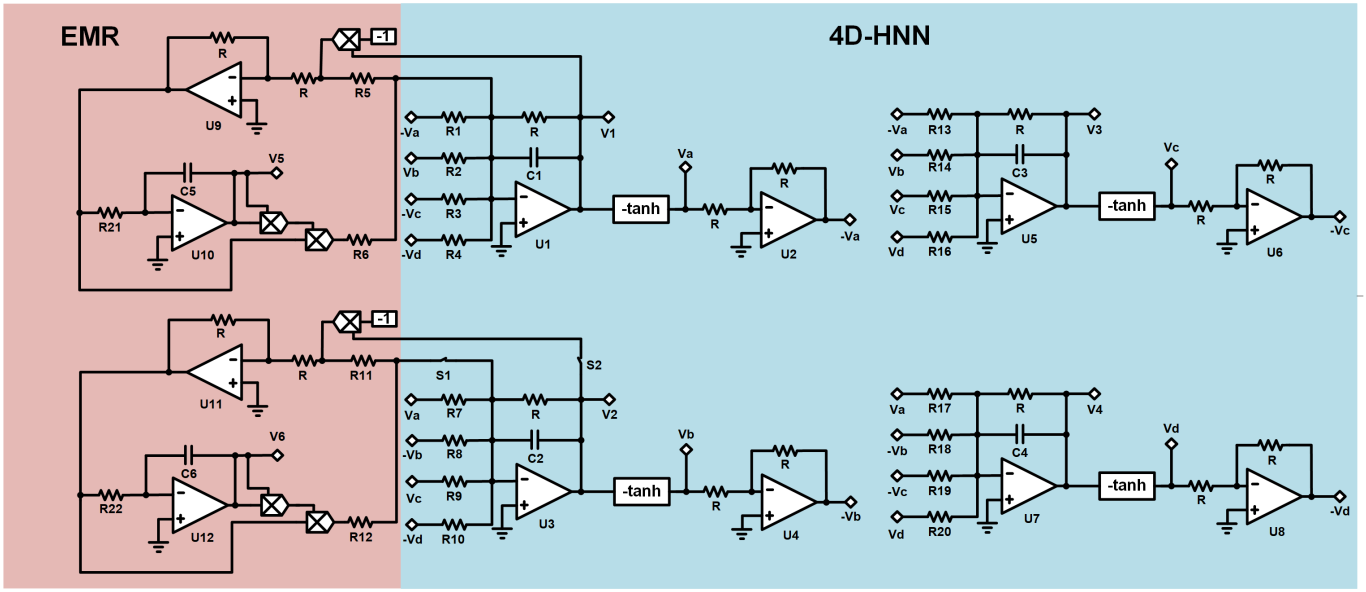

FIG. 17: HNN neural network circuit design.

integral circuit module. $V_1, V_2, V_3, V_4, V_5, V_6$ are denoted as the initial values in the mathematical model, which are the initial voltages on the capacitors of the integral circuit in the basic unit circuit module. In the simulation, the initial values of capacitors C1-C6 in Fig. 17 are set as $(V_1, V_2, V_3, V_4, V_5, V_6) = (0.1, 0, 0, 0, 0, 0)$. The $-V_a$, $-V_b$, $-V_c$, $-V_d$ in the figure are the outputs of the respective circuit module, i.e., the values of V_a, $-V_b$, $-V_c$, and V_d are inverted and outputted by the respective circuit of $1:-1$. The memristor circuit module is connected to the basic unit circuit and consists of two amplifiers and an integral circuit. Several modules are combined with the -tanh circuit module to form the final circuit design.

In the circuit, the resistance of all resistors R is set to $10k\Omega$ and the capacitance of all capacitors C is set to $10nF$, so the value of the circuit time constant RC is $100\mu s$. Based on the system parameters of the HNN, the value of each resistor in the basic unit circuit module is taken as $R_1 = R_3 = R_9 = R_{15} = R_{17} = R_{20} = R/1.5 = 6.6667k\Omega$, $R_2 = R/0.45 = 22.2222k\Omega$, $R_4 = R_{10} = R/1 = 10k\Omega$, $R_{13} = R_{14} = R/2 = 5k\Omega$, $R_{16} = R/10 = 1k\Omega$, $R_{18} = R_{19} = R/0.5 = 20k\Omega$. In addition, the values of the components of the memristor circuit module $R_5 = R_{11} = R/|\alpha\rho|$, $R_6 = R_{12} = R/|3\beta\rho|$, $R_{21} = R/|\mu_1|$, and $R_{22} = R/|\mu_2|$.

Since the parameters of the two EMRs are the same and the rest of the parameters of the EMRs are the same in the two different cases, the memristor parameters in the circuit model are fixed and their associated resistance values in the circuit are fixed, that is, ρ=2, β=-1, and μ=1, $R_6 = R_{12} = 1.6667k\Omega$, $R_{21} = 10k\Omega$ and $R_{22} = 200k\Omega$.When the switches S1, and S2 are fully open, the circuit verifies the chaotic attractor under Case 1. Taking Fig. 7(f) as an example, when parameter α is 1 and the R5 resistance value is $10k\Omega$, the time domain waveform diagram of X_1 is shown in Fig. 18(a), and its phase portrait is shown in Fig. 18(b). When the two switches are turned off, the circuit at this time is impacted by dual EMR. Taking Fig. 13 as an example, when parameter α is 0.75, the time domain waveform diagram of the X_3 is shown in Fig. 18(c), and its phase portrait is shown in Fig. 18(d). Similarly, the dynamical behavior of the neural network under the influence of EMR was verified in FPGA hardware experiments. Numerical computation and timing differences are not considered in the FPGA environment. Results are shown in Fig. 19, where Fig. 19(a) is the environment of FPGA hardware implementation. The periodic and chaotic phenomena under a single EMR in Fig. 19(b-d) are the same as in Fig. 7. The chaotic phenomenon under double EMR in Fig. 19(e, f) is the same as in Fig. 14.

V. CONCLUSION

This paper investigates the chaotic dynamics of HNN under the influence of different amounts of EMR. The cases of a single EMR affecting one neuron and a dual EMR affecting two neurons are presented respectively. Through the study, it is firstly found that the evolution of chaotic phenomena can be seen in the bifurcation and Lyapunov exponents of the four-dimensional HNN under the influence of EMR. Under the influence of dual EMR, the Poincaré map and the time-domain waveform diagrams are analyzed. Chaos and multiperiodic phenomena appeared, and the suppression properties of the dual EMR on system chaos are also analyzed by the maximum Lyapunov exponent. The results show that the external stimulus represented by EMR can affect the inherently chaotic system. It can both make it have more complex dynamical behavior and suppress the complex chaotic behavior. Finally, the feasibility of the theory is verified by circuit experiments and FPGA, and the results of this study have potential applications for the control of chaotic phenomena.

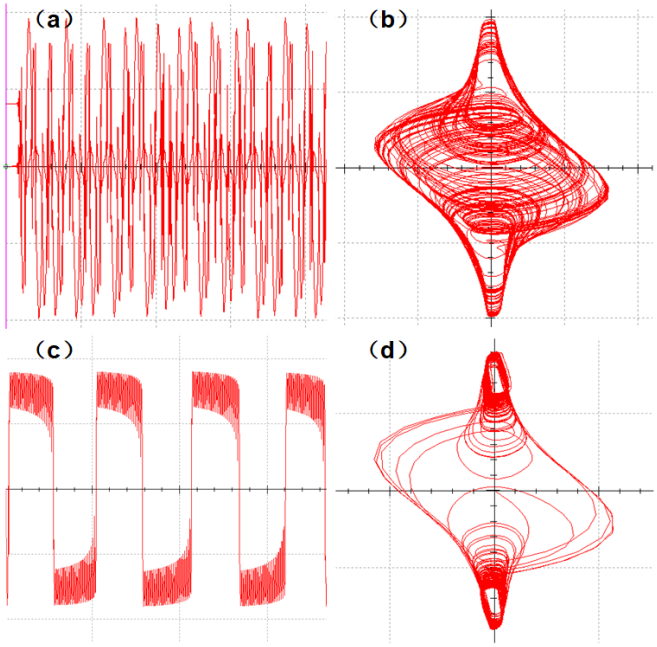

FIG. 18: Time domain waveforms and phase portraits of MULTISIM software simulations. (a) and (b) Chaotic attractor with single EMR; (c) and (d) multiperiodic attractor with dual EMR.

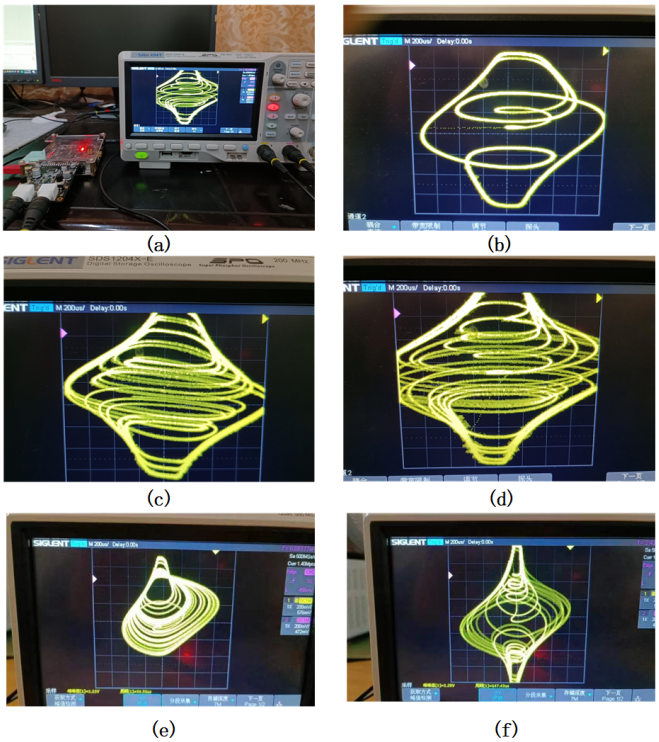

FIG. 19: FPGA hardware implementation. (a) Experimental environment during validation of chaotic phenomena; (b), (c) and (d) period, transient chaos and chaos under single EMR; (e) and (f) chaos under dual EMR.

ACKNOWLEDGMENTS

This work was supported in part by the National Natural Science Foundation of China under Grant No. 62061014, in part by the Natural Science Foundation of Hunan Province under Grant No.2022JJ40514, in part by the Scientific Research Project of Hunan Provincial Department of Education, China under Grant No.23B0318 and 23B1112, in part by Open Fund of Engineering Laboratory of Spatial Information Technology of Highway Geological Disaster Early Warning in Hunan Province, Changsha University of Science & Technology under Grant No.kfj220603, in part by the Open Research Project of the State Key Laboratory of Industrial Control Technology, Zhejiang University, China under Grant No.ICT2023B38, in part by the Practice Innovation and Entrepreneurship Ability Enhancement Plan of Changsha University of Science and Technology Grant No. CLSJCX23102.

AUTHOR DECLARATIONS

Conflict of Interest

The authors have no conflicts to disclose.

Author Contributions

Wei Yao: Methodology (equal); Writing - review & editing (equal). Jia Fang: Conceptualization (equal); Methodology (equal); Software (equal); Writing-original draft (equal); Writing - review & editing (equal). Fei Yu: Conceptualization (equal); Writing - review & editing (equal). Li Xiong: Conceptualization (equal); Supervision (equal); Writing - review & editing (equal). Lihong Tang: Supervision (equal); Writing - review & editing (equal). Jin Zhang: Supervision (equal); Writing - review & editing (equal). Yichuang Sun:Conceptualization (equal); Writing - review & editing (equal).

REFERENCES

[1]O. Sporns, G. Tononi, and G. Edelman, "Connectivity and complexity: the relationship between neuroanatomy and brain dynamics," Neural networks **13**, 909–922 (2000).
[2]O. Sporns, "The complex brain: Connectivity, dynamics, information," Trends in Cognitive Sciences **26**, 1066–1067 (2022).
[3]M. Segarra, M. R. Aburto, and A. Acker-Palmer, "Blood-brain barrier dynamics to maintain brain homeostasis," Trends in neurosciences **44**, 393–405 (2021).
[4]M. Ursino, C. Cuppini, and E. Magosso, "Neurocomputational approaches to modelling multisensory integration in the brain: A review," Neural Networks **60**, 141–165 (2014).
[5]A. Tozzi and L. Mariniello, "Unusual mathematical approaches untangle nervous dynamics," Biomedicines **10**, 2581 (2022).
[6]W. Yao, C. Wang, Y. Sun, and C. Zhou, "Robust multimode function synchronization of memristive neural networks with parameter perturbations and time-varying delays," IEEE Transactions on Systems, Man, and Cybernetics: Systems **52**, 260–274 (2020).

[7]W. Nicola, P. J. Hellyer, S. A. Campbell, and C. Clopath, "Chaos in homeostatically regulated neural systems," Chaos: An Interdisciplinary Journal of Nonlinear Science **28** (2018).
[8]S. Kong, C. Li, S. He, S. Çiçek, and Q. Lai, "A memristive map with coexisting chaos and hyperchaos," Chinese Physics B **30**, 110502 (2021).
[9]W. Yao, K. Gao, Z. Zhang, L. Cui, and J. Zhang, "An image encryption algorithm based on a 3d chaotic hopfield neural network and random row–column permutation," Frontiers in Physics **11**, 1162887 (2023).
[10]Q. Lai and L. Yang, "Discrete memristor applied to construct neural networks with homogeneous and heterogeneous coexisting attractors," Chaos, Solitons & Fractals **174**, 113807 (2023).
[11]W. Mo and H. Bao, "Finite-time synchronization for fractional-order quaternion-valued coupled neural networks with saturated impulse," Chaos, Solitons & Fractals **164**, 112714 (2022).
[12]W. Yao, C. Wang, Y. Sun, C. Zhou, and H. Lin, "Exponential multistability of memristive cohen-grossberg neural networks with stochastic parameter perturbations," Applied Mathematics and Computation **386**, 125483 (2020).
[13]S. Zhu and H. Bao, "Event-triggered synchronization of coupled memristive neural networks," Applied Mathematics and Computation **415**, 126715 (2022).
[14]J. J. Hopfield, "Neural networks and physical systems with emergent collective computational abilities," Proceedings of the National Academy of Sciences of the United States of America **79**, 2554–2558 (1982).
[15]M. Chen, C. Chen, B. Bao, and Q. Xu, "Initial sensitive dynamics in memristor synapse-coupled hopfield neural network," Journal of Electronics & Information Technology **42**, 870–877 (2020).
[16]C. Chen, F. Min, F. Hu, J. Cai, and Y. Zhang, "Analog/digital circuit simplification for hopfield neural network," Chaos, Solitons & Fractals **173**, 113727 (2023).
[17]C. Chen, F. Min, Y. Zhang, and H. Bao, "Relu-type hopfield neural network with analog hardware implementation," Chaos, Solitons & Fractals **167**, 113068 (2023).
[18]Y. Guo, M. Lv, C. Wang, and J. Ma, "Energy controls wave propagation in a neural network with spatial stimuli," Neural Networks **171**, 1–13 (2024).
[19]P. Ji, J. Ye, Y. Mu, W. Lin, Y. Tian, C. Hens, M. Perc, Y. Tang, J. Sun, and J. Kurths, "Signal propagation in complex networks," Physics reports **1017**, 1–96 (2023).
[20]B. Yan, F. Parastesh, S. He, K. Rajagopal, S. Jafari, and M. Perc, "Interlayer and intralayer synchronization in multiplex fractional-order neuronal networks," Fractals **30**, 2240194 (2022).
[21]Y. Guo, Y. Xie, and J. Ma, "Nonlinear responses in a neural network under spatial electromagnetic radiation," Physica A: Statistical Mechanics and its Applications **626**, 129120 (2023).
[22]F. Parastesh, M. Mehrabbeik, K. Rajagopal, S. Jafari, and M. Perc, "Synchronization in hindmarsh-rose neurons subject to higher-order interactions," Chaos: An Interdisciplinary Journal of Nonlinear Science **32** (2022).
[23]S. Majhi, M. Perc, and D. Ghosh, "Dynamics on higher-order networks: A review," Journal of the Royal Society Interface **19**, 20220043 (2022).
[24]L. Cui, W. Luo, and Q. Ou, "Analysis of basins of attraction of new coupled hidden attractor system," Chaos, Solitons & Fractals **146**, 110913 (2021).
[25]P. Grassberger and I. Procaccia, "Characterization of strange attractors," Physical review letters **50**, 346 (1983).
[26]P. Grassberger, "Generalized dimensions of strange attractors," Physics letters A **97**, 227–230 (1983).
[27]H. Hentschel and I. Procaccia, "The infinite number of generalized dimensions of fractals and strange attractors," Physica D: Nonlinear Phenomena **8**, 435–444 (1983).
[28]L. Cui, M. Lu, Q. Ou, H. Duan, and W. Luo, "Analysis and circuit implementation of fractional order multi-wing hidden attractors," Chaos, Solitons & Fractals **138**, 109894 (2020).
[29]J. M. T. Thompson and H. B. Stewart, *Nonlinear dynamics and chaos* (John Wiley & Sons, 2002).
[30]S. Boccaletti, C. Grebogi, Y.-C. Lai, H. Mancini, and D. Maza, "The control of chaos: theory and applications," Physics reports **329**, 103–197 (2000).
[31]Y. Zhou, Z. Hua, C.-M. Pun, and C. L. Philip Chen, "Cascade chaotic system with applications," IEEE transactions on cybernetics **45**, 2001–2012 (2015).
[32]X. Peng, Y. Zeng, M. Wang, and Z. Li, "Generating multi-layer nested chaotic attractor and its fpga implementation," Chinese Physics B **30**, 060509 (2021).
[33]Z. Yao, K. Sun, and S. He, "Dynamics of fractional-order chaotic rocard relaxation econometric system," International Journal of Bifurcation and Chaos **32**, 2250195 (2022).
[34]W. Yao, J. Liu, Y. Sun, J. Zhang, F. Yu, L. Cui, and H. Lin, "Dynamics analysis and image encryption application of hopfield neural network with a novel multistable and highly tunable memristor," Nonlinear Dynamics **112**, 693–708 (2024).
[35]N. Novelli, P. Belardinelli, and S. Lenci, "Piecewise integrable neural network: An interpretable chaos identification framework," Chaos: An Interdisciplinary Journal of Nonlinear Science **33** (2023).
[36]H. Lin, C. Wang, J. Sun, X. Zhang, Y. Sun, and H. H. Iu, "Memristor-coupled asymmetric neural networks: Bionic modeling, chaotic dynamics analysis and encryption application," Chaos, Solitons & Fractals **166**, 112905 (2023).
[37]Q. Lai, C. Lai, P. D. K. Kuate, C. Li, and S. He, "Chaos in a simplest cyclic memristive neural network," International Journal of Bifurcation and Chaos **32**, 2250042 (2022).
[38]E. N. Lorenz, "Maximum simplification of the dynamic equations," Tellus **12**, 243–254 (1960).
[39]E. N. Lorenz, "Deterministic nonperiodic flow," Journal of atmospheric sciences **20**, 130–141 (1963).
[40]H. Lin, C. Wang, F. Yu, C. Xu, Q. Hong, W. Yao, and Y. Sun, "An extremely simple multiwing chaotic system: dynamics analysis, encryption application, and hardware implementation," IEEE Transactions on Industrial Electronics **68**, 12708–12719 (2020).
[41]A. Qi, B. Zhu, and G. Wang, "Complex dynamic behaviors in hyperbolic-type memristor-based cellular neural network," Chinese Physics B **31**, 020502 (2022).
[42]A. Wu, J. Zhang, and Z. Zeng, "Dynamic behaviors of a class of memristor-based hopfield networks," Physics Letters A **375**, 1661–1665 (2011).
[43]Z. T. Njitacke, S. D. Isaac, J. Kengne, A. N. Negou, and G. D. Leutcho, "Extremely rich dynamics from hyperchaotic hopfield neural network: Hysteretic dynamics, parallel bifurcation branches, coexistence of multiple stable states and its analog circuit implementation," The European Physical Journal Special Topics **229**, 1133–1154 (2020).
[44]W. Yao, C. Wang, Y. Sun, S. Gong, and H. Lin, "Event-triggered control for robust exponential synchronization of inertial memristive neural networks under parameter disturbance," Neural Networks **164**, 67–80 (2023).
[45]Z. Xie, J. Sun, Y. Tang, X. Tang, O. Simpson, and Y. Sun, "A k-svd based compressive sensing method for visual chaotic image encryption," Mathematics **11**, 1658 (2023).
[46]X. Ge, C. Li, Y. Li, C. Yi, and H. Fu, "A hyperchaotic map with distance-increasing pairs of coexisting attractors and its application in the pelican optimization algorithm," Chaos, Solitons & Fractals **173**, 113636 (2023).
[47]J. Ma and J. Tang, "A review for dynamics of collective behaviors of network of neurons," Science China Technological Sciences **58**, 2038–2045 (2015).
[48]M. Lv, C. Wang, G. Ren, J. Ma, and X. Song, "Model of electrical activity in a neuron under magnetic flow effect," Nonlinear dynamics **85**, 1479–1490 (2016).
[49]Q. Wan, Z. Yan, F. Li, S. Chen, and J. Liu, "Complex dynamics in a hopfield neural network under electromagnetic induction and electromagnetic radiation," Chaos: An Interdisciplinary Journal of Nonlinear Science **32**, 073107 (2022).
[50]Q. Wan, Z. Yan, F. Li, J. Liu, and S. Chen, "Multistable dynamics in a hopfield neural network under electromagnetic radiation and dual bias currents," Nonlinear Dynamics **109**, 2085–2101 (2022).
[51]H. Lin, C. Wang, W. Yao, and Y. Tan, "Chaotic dynamics in a neural network with different types of external stimuli," Communications in Nonlinear Science and Numerical Simulation **90**, 105390 (2020).
[52]H. Lin and C. Wang, "Influences of electromagnetic radiation distribution on chaotic dynamics of a neural network," Applied Mathematics and Computation **369**, 124840 (2020).
[53]S. Xu, X. Wang, and X. Ye, "A new fractional-order chaos system of hopfield neural network and its application in image encryption," Chaos, Solitons & Fractals **157**, 111889 (2022).

[54]R. Qiu, Y. Dong, X. Jiang, and G. Wang, "Two-neuron based memristive hopfield neural network with synaptic crosstalk," Electronics **11**, 3034 (2022).
[55]W. Yao, F. Yu, J. Zhang, and L. Zhou, "Asymptotic synchronization of memristive cohen-grossberg neural networks with time-varying delays via event-triggered control scheme," Micromachines **13**, 726 (2022).
[56]J. J. Hopfield, "Neurons with graded response have collective computational properties like those of two-state neurons," Proceedings of the national academy of sciences **81**, 3088–3092 (1984).
[57]M. Lv and J. Ma, "Multiple modes of electrical activities in a new neuron model under electromagnetic radiation," Neurocomputing **205**, 375–381 (2016).
[58]S. H. Strogatz, *Nonlinear dynamics and chaos: with applications to physics, biology, chemistry, and engineering* (CRC press, 2018).
[59]T. Tél, "The joy of transient chaos," Chaos: An Interdisciplinary Journal of Nonlinear Science **25**, 097619 (2015).
[60]F. Yu, Y. Yuan, C. Wu, W. Yao, C. Xu, S. Cai, and C. Wang, "Modeling and hardware implementation of a class of hamiltonian conservative chaotic systems with transient quasi-period and multistability," Nonlinear Dynamics **112**, 2331–2347 (2024).
[61]L. Chua, "Memristor-the missing circuit element," IEEE Transactions on circuit theory **18**, 507–519 (1971).
[62]S. Duan and X. Liao, "An electronic implementation for liao's chaotic delayed neuron model with non-monotonous activation function," Physics Letters A **369**, 37–43 (2007).
[63]S. Duan and L. Wang, "A novel delayed chaotic neural model and its circuitry implementation," Computers & Mathematics with Applications **57**, 1736–1742 (2009).